

# Unified CFD approach to simulate two-phase flows in presence of surface forces

Vladimir V. Chudanov, Anna E. Aksenova and Alex A. Leonov

**Abstract**— In this paper the diffuse interface model for direct numerical simulation of liquid-vapor interfaces in the presence of surface is presented. This model is developed from two-phase compressible flow approaches known as relaxation-projection method for compressible flows, simple and efficient relaxation method using pressure non-equilibrium model. The model accounts for the phase compressibility and surface tension effects and adapted for simulation of the bubble and drop flows. Results of testing of numerical technique are presented and demonstrate the good perspective of developed approach for simulation of multi-phase flows.

**Keywords**— CFD, relaxation-projection method, surface force, two-phase flows.

## I. INTRODUCTION

THE liquid-vapor flows with phase change are often encountered in industrial applications such as nuclear reactors, heat exchangers, boilers, etc. Their better understanding requires experimental investigations as well as the development of analytical models. To develop analytical models and to help interpret experimental data and understand local physical phenomena the direct numerical simulations can be used. The use of the direct numerical simulation is already quite common in single-phase fluid dynamics. The numerical problems encountered to simulate two-phase flows with phase change are much more complicated. The tracking of a surface of discontinuity on a fixed numerical grid is a base complexity in these numerical problems. Several methods proved their efficiency to solve this problem; the most common ones are the volume-of-fluid [1], front-tracking [2], and level-set methods [3]. These methods mainly deal with immiscible fluid systems. In such systems, the speed of displacement of an interface is equal to the velocity of the fluids (gas and liquid) at the interface. Therefore, knowing the velocity field, it is quite easy to interpolate it at the interface and move the

interface accordingly. When phase change exists, the problem is more complicated because three different velocities exist at an interface: the velocities of the liquid and vapor phases and the speed of displacement of the interface.

Liquid-vapor phase change effects have been resolved within the one-fluid formulation by different researchers: Beux with colleagues [4] used the LS method; Jamet [5] applied the so-called second gradient theory or the Cahn-Hilliard equations.

During of the last ten years numerical methods and algorithms for solving of the heat and mass transfer problems in compressible/incompressible fluids were developed. Among these are algorithms for solving of incompressible fluid dynamics, algorithms for solving of compressible fluid dynamics at the low Mach numbers, the monotone multi-dimensional schemes for solving of an advection equation, an effective algorithm for solving of elliptical equation for pressure correction. These methods and algorithms were applied successfully for computational support of the experiments financed by Nuclear Energy Agency at Organization of Economic Cooperation and Development within the MASCA project [6], where a behavior of the two non-mixing liquids, such as corium and steel was investigated. Now these computing tools will be extended on a case of two-phase flows as a gas-liquid system.

For incompressible/compressible two-phase flows unified CFD approach was developed [7] which is based on the developed algorithms with small scheme diffusion, where the discrete approximations are constructed with use of finite-volume methods and fully staggered grids. For modeling of 3D turbulent single-phase flows LES approach (commutative filters) was used. For modeling of 3D turbulent two-phase flows by means DNS the enough detailed grids and effective numerical methods developed in IBRAE for solving of CFD problems were applied. For observation of an interface of two-phase flow the modified VOF methods and multidimensional transfer schemas of TVD-type with small scheme diffusion with use of sub-grid simulation were used.

A considerable number of modern simulation methods of multiphase and multicomponents gas dynamics flows are based on the numerical solution of Euler or the Navier-Stokes equations which are usually supplemented by one or several equations expressing conservation laws of specific physical values to given problem (concentration of gas bubbles), it is

V. V. Chudanov is with the Nuclear Safety Institute (IBRAE) of Russian Academy of Sciences, 52, Bolshaya Tulkaya street, Moscow, 115191, Russia (corresponding author to provide phone: +7-495-955-22-34; e-mail: chud@ibrae.ac.ru).

A. E. Aksenova is with the Nuclear Safety Institute (IBRAE) of Russian Academy of Sciences, 52, Bolshaya Tulkaya street, Moscow, 115191, Russia (corresponding author to provide phone: +7-495-955-22-34; e-mail: aks@ibrae.ac.ru).

A. A. Leonov is with the Nuclear Safety Institute (IBRAE) of Russian Academy of Sciences, 52, Bolshaya Tulkaya street, Moscow, 115191, Russia (corresponding author to provide phone: +7-495-955-22-34; e-mail: leon@ibrae.ac.ru).

necessary for definition of interface parameters for multiphase system.

Application of such numerical methods leads to occurrence of artificial diffusivity through contact discontinuity and to artificial mixing of substances on interface. In such artificial mix of value of all thermodynamic parameters are calculated with an error. With strongly differing parameters of substances such approach leads to negative values of pressure already on the second step on time. The two-phase model has been offered in Abgral and Saurel's paper [8], which allowing defining thermodynamic and kinetic variables of each component of a mix. Thus in any place of a calculated grid the identical equations were solved by means of the same numerical method as for a case of two not mixing components separated by an interface, and for a case of presence of physical mixing of various substances.

The diffuse interface model for direct numerical simulation of liquid-vapor interfaces in the presence of surface forces was developed from two-phase compressible flow approaches known as relaxation-projection method for compressible flows, simple and efficient relaxation method using pressure non-equilibrium model. The model accounts both the phase compressibility and surface tension effects and adapted for simulation of the bubble and drop flows. Results of testing of numerical technique speak about the good perspective of developed approach for simulation of multi-phase flows.

The possibility of using diffuse interface model for direct numerical simulation of liquid-vapor interfaces in the presence of surface forces is used to test numerical technique. This model was developed by using Hamilton's principle of stationary action [9]. Numerical technique is based on adapted HLLC Riemann solver [10] supplemented with simple and efficient relaxation method using pressure non-equilibrium model [11]. Such approach was used for simulation of the bubble and drop flows.

Generalization for phase transition modeling can be achieved by natural physical processes splitting with relaxation and phase transition [12].

## II. MODEL DESCRIPTION

For the mixture Lagrangian

$$L = \rho \left( \frac{|\bar{u}|^2}{2} - \varepsilon \right) - \frac{\lambda}{m} |\nabla \phi|^m,$$

where  $\bar{u}$  - velocity;  $\rho$  - mixture density,  $\rho = \alpha_1 \rho_1 + \alpha_2 \rho_2$ ;

$\varepsilon$  - mixture specific internal energy,

$\varepsilon = \frac{\alpha_1 \rho_1}{\rho} \varepsilon_1 + \frac{\alpha_2 \rho_2}{\rho} \varepsilon_2 = y_1 \varepsilon_1 + y_2 \varepsilon_2$ ;  $\lambda$  - capillarity

parameter;  $\phi$  - Heaviside step function;  $m$  - interface sharpness parameter ( $m=1$  for sharp interface), Hamilton principle allows obtaining the following system of equations governing two compressible fluids in mechanical equilibrium with capillary effects [12]:

$$\left\{ \begin{aligned} \frac{\partial \alpha_1}{\partial t} + \bar{u} \times \nabla \alpha_1 &= \frac{\rho_2 c_2^2 - \rho_1 c_1^2}{\alpha_1 c_1^2 + \rho_2 c_2^2} \times \nabla \bar{u}; \\ \frac{\partial \rho}{\partial t} + \text{div}(\rho \bar{u}) &= 0; \\ \frac{\partial (y_2)}{\partial t} + \bar{u} \nabla y_2 &= 0; \\ \frac{\partial (\phi)}{\partial t} + \bar{u} \nabla \phi &= 0; \\ \frac{\partial (\rho \bar{u})}{\partial t} + \text{div} \left( \rho \bar{u}_k \otimes \bar{u}_k + P - \lambda |\nabla \phi|^m \times \left( I - \frac{\nabla \phi}{|\nabla \phi|} \otimes \frac{\nabla \phi}{|\nabla \phi|} \right) \right) &= 0; \\ P &= p + \lambda \frac{m-1}{m} |\nabla \phi|^m; \\ \frac{\partial \left( \rho \left( \frac{|\bar{u}|^2}{2} + E \right) \right)}{\partial t} + \text{div} \left( \rho \bar{u} \times \left( E + \frac{|\bar{u}|^2}{2} \right) + \bar{u} P - \bar{u} \times \lambda |\nabla \phi|^m \times \left( I - \frac{\nabla \phi}{|\nabla \phi|} \otimes \frac{\nabla \phi}{|\nabla \phi|} \right) \right) &= 0; \\ E &= \varepsilon + \frac{\lambda}{\rho m} |\nabla \phi|^m. \end{aligned} \right. \quad (1)$$

The order parameter  $\phi$  can be identified with the mass fraction:

$$\bar{w} = \nabla \phi = \nabla y_2. \quad (2)$$

For sharp liquid-vapor interfaces ( $m = 1$ ) system (1) in two-dimensional case puts on:

$$\left\{ \begin{aligned} \frac{\partial \alpha_1}{\partial t} + \bar{u} \times \nabla \alpha_1 &= \frac{\rho_2 c_2^2 - \rho_1 c_1^2}{\alpha_1 c_1^2 + \rho_2 c_2^2} \times \nabla \bar{u}; \\ \frac{\partial \rho}{\partial t} + \text{div}(\rho \bar{u}) &= 0; \\ \frac{\partial (\rho y_2)}{\partial t} + \text{div}(\rho y_2 \bar{u}) &= 0; \\ \frac{\partial \bar{w}}{\partial t} + \text{div}(\bar{w} \bar{u}) &= 0; \\ \frac{\partial (\rho u_x)}{\partial t} + \frac{\partial \left( \rho u_x^2 + p - \lambda w \times \left( 1 - \frac{w_x^2}{w^2} \right) \right)}{\partial x} + \frac{\partial \left( \rho u_x u_y + \lambda \frac{w_x w_y}{w} \right)}{\partial y} &= 0; \\ \frac{\partial (\rho u_y)}{\partial t} + \frac{\partial \left( \rho u_x u_y + \lambda \frac{w_x w_y}{w} \right)}{\partial x} + \frac{\partial \left( \rho u_y^2 + p - \lambda w \times \left( 1 - \frac{w_y^2}{w^2} \right) \right)}{\partial y} &= 0; \\ \frac{\partial \left( \rho \left( \varepsilon + \frac{|\bar{u}|^2}{2} \right) + \lambda |\bar{w}| \right)}{\partial t} + \text{div} \left( \rho \bar{u} \times \left( \varepsilon + \frac{|\bar{u}|^2}{2} \right) + \bar{u} \lambda |\bar{w}| + \bar{u} p \right) + \\ &+ \frac{\partial \left( \frac{u_x \lambda w_x}{w} \times (w_x + w_y) \right)}{\partial x} + \frac{\partial \left( \frac{u_y \lambda w_y}{w} \times (w_x + w_y) \right)}{\partial y} = 0. \end{aligned} \right. \quad (3)$$

The hyperbolicity of the model (3) is shown in [12].

To solve it numerically several disadvantages have to be taken into account [11].

Main among these disadvantages concerns with non monotone behavior of the equilibrium sound speed with respect to the volume fraction.

Also non-conservative volume fraction equation could yield to positivity preserving difficulties when rarefaction or compression waves are present at interfaces.

To avoid such disadvantages pressure non-equilibrium model is used. With this approach system (3) will take form:

$$\begin{cases}
 \frac{\partial \alpha_1}{\partial t} + \bar{u} \times \nabla \alpha_1 = \mu(p_1 - p_2); \\
 \frac{\partial \rho}{\partial t} + \text{div}(\rho \bar{u}) = 0; \\
 \frac{\partial (\rho y_2)}{\partial t} + \text{div}(\rho y_2 \bar{u}) = 0; \\
 \frac{\partial \bar{w}}{\partial t} + \text{div}(\bar{w} \bar{u}) = 0; \\
 \frac{\partial (\rho u_x)}{\partial t} + \frac{\partial \left( \rho u_x^2 + \alpha_1 p_1 + \alpha_2 p_2 - \lambda w \times \left( 1 - \frac{w_x^2}{w^2} \right) \right)}{\partial x} + \frac{\partial \left( \rho u_x u_y + \lambda \frac{w_x w_y}{w} \right)}{\partial y} = 0; \\
 \frac{\partial (\rho u_y)}{\partial t} + \frac{\partial \left( \rho u_x u_y + \lambda \frac{w_x w_y}{w} \right)}{\partial x} + \frac{\partial \left( \rho u_y^2 + \alpha_1 p_1 + \alpha_2 p_2 - \lambda w \times \left( 1 - \frac{w_y^2}{w^2} \right) \right)}{\partial y} = 0; \\
 \frac{\partial (\alpha_1 \rho_1 e_1)}{\partial t} + \text{div}(\alpha_1 \rho_1 e_1 \bar{u}) + \alpha_1 p_1 \text{div} \bar{u} = -p_1 \mu \times (p_1 - p_2); \\
 \frac{\partial (\alpha_2 \rho_2 e_2)}{\partial t} + \text{div}(\alpha_2 \rho_2 e_2 \bar{u}) + \alpha_2 p_2 \text{div} \bar{u} = p_1 \mu \times (p_1 - p_2).
 \end{cases} \quad (4)$$

where  $p_I$  – interface pressure.

At first step the hyperbolic part of the system (4) is solved:

$$\begin{cases}
 \frac{\partial \alpha_1}{\partial t} + \bar{u} \times \nabla \alpha_1 = 0; \\
 \frac{\partial \rho}{\partial t} + \text{div}(\rho \bar{u}) = 0; \\
 \frac{\partial (\rho y_2)}{\partial t} + \text{div}(\rho y_2 \bar{u}) = 0; \\
 \frac{\partial \bar{w}}{\partial t} + \text{div}(\bar{w} \bar{u}) = 0; \\
 \frac{\partial (\rho u_x)}{\partial t} + \frac{\partial \left( \rho u_x^2 + \alpha_1 p_1 + \alpha_2 p_2 - \lambda w \times \left( 1 - \frac{w_x^2}{w^2} \right) \right)}{\partial x} + \frac{\partial \left( \rho u_x u_y + \lambda \frac{w_x w_y}{w} \right)}{\partial y} = 0; \\
 \frac{\partial (\rho u_y)}{\partial t} + \frac{\partial \left( \rho u_x u_y + \lambda \frac{w_x w_y}{w} \right)}{\partial x} + \frac{\partial \left( \rho u_y^2 + \alpha_1 p_1 + \alpha_2 p_2 - \lambda w \times \left( 1 - \frac{w_y^2}{w^2} \right) \right)}{\partial y} = 0; \\
 \frac{\partial (\alpha_1 \rho_1 e_1)}{\partial t} + \text{div}(\alpha_1 \rho_1 e_1 \bar{u}) + \alpha_1 p_1 \text{div} \bar{u} = 0; \\
 \frac{\partial (\alpha_2 \rho_2 e_2)}{\partial t} + \text{div}(\alpha_2 \rho_2 e_2 \bar{u}) + \alpha_2 p_2 \text{div} \bar{u} = 0.
 \end{cases} \quad (5)$$

Next relaxation step forces the solution of pressure non-equilibrium model (5) to converge to that of the equilibrium model (3). This step is fulfilled for the system:

$$\begin{cases}
 \frac{\partial \alpha_1}{\partial t} = \mu(p_1 - p_2); \\
 \frac{\partial \rho}{\partial t} = 0; \\
 \frac{\partial (\rho y_2)}{\partial t} = 0; \\
 \frac{\partial \bar{w}}{\partial t} = 0; \\
 \frac{\partial (\rho u_x)}{\partial t} = 0; \\
 \frac{\partial (\rho u_y)}{\partial t} = 0; \\
 \frac{\partial (\alpha_1 \rho_1 e_1)}{\partial t} = -p_1 \mu \times (p_1 - p_2); \\
 \frac{\partial (\alpha_2 \rho_2 e_2)}{\partial t} = p_1 \mu \times (p_1 - p_2).
 \end{cases} \quad (6)$$

### III. NUMERICAL TECHNIQUE

The main point is that the numerical algorithm does not look for the liquid-vapor interfaces, and it is identical in the whole calculated region.

In the absence of relaxation terms the conservative part of system (5) are updated with conversational Godunov scheme:

$$\begin{aligned}
 U_{i,j}^{n+1} &= U_{i,j}^n - \frac{\Delta t}{\Delta x} \left( F_x^*(U_{i+1,j}^n, U_{i,j}^n) - F_x^*(U_{i,j}^n, U_{i-1,j}^n) \right) - \\
 &\quad - \frac{\Delta t}{\Delta y} \left( F_y^*(U_{i,j+1}^n, U_{i,j}^n) - F_y^*(U_{i,j}^n, U_{i,j-1}^n) \right),
 \end{aligned}$$

where upper script \* stands for the perturbed state,

$$U = \left( \rho, \rho y_2, w_x, w_y, \rho u_x, \rho u_y \right)$$

$$\begin{aligned}
 F_x &= \left( \rho u_x, \rho y_2 u_x, w_x u_x + w_y u_y, \rho u_x^2 + \alpha_1 p_1 + \alpha_2 p_2 - \right. \\
 &\quad \left. - \lambda w \times \left( 1 - \frac{w_x^2}{w^2} \right), \rho u_x u_y + \lambda \frac{w_x w_y}{w} \right),
 \end{aligned}$$

$$\begin{aligned}
 F_y &= \left( \rho u_y, \rho y_2 u_y, w_x u_x + w_y u_y, \rho u_x u_y + \lambda \frac{w_x w_y}{w}, \rho u_y^2 + \right. \\
 &\quad \left. + \alpha_1 p_1 + \alpha_2 p_2 - \lambda w \times \left( 1 - \frac{w_y^2}{w^2} \right) \right).
 \end{aligned}$$

The volume fraction is calculated using the Godunov method for advection equation that guarantees volume fraction positivity during the hyperbolic step:

$$\begin{aligned}
 (\alpha_1)_{i,j}^{n+1} &= (\alpha_1)_{i,j}^n - \frac{\Delta t}{\Delta x} \left( (u_x \alpha_1)_{i+\frac{1}{2},j}^* - (u_x \alpha_1)_{i-\frac{1}{2},j}^* - \right. \\
 &\quad \left. - (\alpha_1)_{i,j}^n \times \left( (u_x)_{i+\frac{1}{2},j}^* - (u_x)_{i-\frac{1}{2},j}^* \right) \right) - \\
 &\quad - \frac{\Delta t}{\Delta y} \left( (u_y \alpha_1)_{i,j+\frac{1}{2}}^* - (u_y \alpha_1)_{i,j-\frac{1}{2}}^* - \right. \\
 &\quad \left. - (\alpha_1)_{i,j}^n \times \left( (u_y)_{i,j+\frac{1}{2}}^* - (u_y)_{i,j-\frac{1}{2}}^* \right) \right).
 \end{aligned}$$

The non-conservative energy equations are updated with simplest approximation by assuming the product  $(\alpha_k \rho_k)_{i,j}^n$  constant during time step:

$$\begin{aligned}
 (\alpha_k \rho_k e_k)_{i,j}^{n+1} &= (\alpha_k \rho_k e_k)_{i,j}^n - \\
 &\quad - \frac{\Delta t}{\Delta x} \left( (\alpha_k \rho_k e_k)_{i+\frac{1}{2},j}^* - (\alpha_k \rho_k e_k)_{i-\frac{1}{2},j}^* - \right. \\
 &\quad \left. - (\alpha_k \rho_k)_{i,j}^n \times \left( (u_x)_{i+\frac{1}{2},j}^* - (u_x)_{i-\frac{1}{2},j}^* \right) \right) - \\
 &\quad - \frac{\Delta t}{\Delta y} \left( (\alpha_k \rho_k e_k)_{i,j+\frac{1}{2}}^* - (\alpha_k \rho_k e_k)_{i,j-\frac{1}{2}}^* - \right. \\
 &\quad \left. - (\alpha_k \rho_k)_{i,j}^n \times \left( (u_y)_{i,j+\frac{1}{2}}^* - (u_y)_{i,j-\frac{1}{2}}^* \right) \right).
 \end{aligned}$$

The lack of accuracy in the internal energy computation will be corrected on the relaxation step in agreement with the second law of thermodynamics.

To determine the values of thermodynamic variables for perturbed state the adaptation of HLLC solver was performed. The left- and right- facing waves speeds along X and Y directions are obtained as following:

$$\begin{aligned}
 (S_L)_x &= \max((u_x)_L - (c_x)_L, (u_x)_R - (c_x)_R), \\
 (S_L)_y &= \max((u_y)_L - (c_y)_L, (u_y)_R - (c_y)_R), \\
 (S_R)_x &= \max((u_x)_L + (c_x)_L, (u_x)_R + (c_x)_R), \\
 (S_R)_y &= \max((u_y)_L + (c_y)_L, (u_y)_R + (c_y)_R),
 \end{aligned}$$

where  $c^2 = y_1^2 c_1^2 + y_2^2 c_2^2$  – frozen sound speed.

The speeds of intermediate waves or contact discontinuities are estimated as:

$$u_x^* = (S_M)_x = \left\{ \left( \rho u_x^2 + p - \lambda w \times \left( 1 - \frac{w_x^2}{w^2} \right) \right)_L - \left( \rho u_x^2 + p - \lambda w \times \left( 1 - \frac{w_x^2}{w^2} \right) \right)_R - (S_L)_x \rho_L (u_x)_L + (S_R)_x \rho_R (u_x)_R \right\} / \left\{ (\rho u_x)_L - (\rho u_x)_R - (S_L)_x \rho_L + (S_R)_x \rho_R \right\} \quad (7)$$

$$u_y^* = (S_M)_y = \left\{ \left( \rho u_y^2 + p - \lambda w \times \left( 1 - \frac{w_y^2}{w^2} \right) \right)_L - \left( \rho u_y^2 + p - \lambda w \times \left( 1 - \frac{w_y^2}{w^2} \right) \right)_R - (S_L)_y \rho_L (u_y)_L + (S_R)_y \rho_R (u_y)_R \right\} / \left\{ (\rho u_y)_L - (\rho u_y)_R - (S_L)_y \rho_L + (S_R)_y \rho_R \right\} \quad (8)$$

From above wave speeds the variable states are determined:

$$\begin{aligned} (\rho_R^*)_x &= (\rho_R)_x \times \frac{(S_R)_x - (u_x)_R}{(S_R)_x - (S_M)_x}, \\ (\rho_L^*)_x &= (\rho_L)_x \times \frac{(S_L)_x - (u_x)_L}{(S_L)_x - (S_M)_x}, \\ (\rho_R^*)_y &= (\rho_R)_y \times \frac{(S_R)_y - (u_y)_R}{(S_R)_y - (S_M)_y}, \\ (\rho_L^*)_y &= (\rho_L)_y \times \frac{(S_L)_y - (u_y)_L}{(S_L)_y - (S_M)_y}. \end{aligned} \quad (9)$$

$$\begin{aligned} (w_x)_R^* &= (w_x)_R \times \frac{(\rho_R^*)_x}{(\rho_R)_x}, \\ (w_x)_L^* &= (w_x)_L \times \frac{(\rho_L^*)_x}{(\rho_L)_x}, \end{aligned} \quad (10)$$

$$\begin{aligned} (w_y)_R^* &= (w_y)_R, \\ (w_y)_L^* &= (w_y)_L, \\ (w_x)_R^* &= (w_x)_R, \\ (w_x)_L^* &= (w_x)_L, \\ (w_y)_R^* &= (w_y)_R \times \frac{(\rho_R^*)_y}{(\rho_R)_y}, \\ (w_y)_L^* &= (w_y)_L \times \frac{(\rho_L^*)_y}{(\rho_L)_y}. \end{aligned} \quad (11)$$

$$\begin{aligned} p_x^* &= (p_R)_x + (\rho_R)_x \times (u_x)_R \times \\ &\times \left( \left( (u_x)_R \right)_x - (S_R)_x \right) + (\rho_R^*)_x \times (S_M)_x \left( (S_R)_x - (S_M)_x \right) + \\ &+ \lambda \times (w_R^*)_x \times \left( 1 - \frac{(w_x)_R^2}{(w_R^*)_x^2} \right) - \lambda \times (w_R)_x \times \left( 1 - \frac{(w_x)_R^2}{(w_R)_x^2} \right); \end{aligned} \quad (12)$$

$$\begin{aligned} p_y^* &= (p_R)_y + (\rho_R)_y \times (u_y)_R \times \\ &\times \left( \left( (u_y)_R \right)_y - (S_R)_y \right) + (\rho_R^*)_y \times (S_M)_y \left( (S_R)_y - (S_M)_y \right) + \\ &+ \lambda \times (w_R^*)_y \times \left( 1 - \frac{(w_y)_R^2}{(w_R^*)_y^2} \right) - \lambda \times (w_R)_y \times \left( 1 - \frac{(w_y)_R^2}{(w_R)_y^2} \right). \end{aligned} \quad (13)$$

The volume fraction jump is constant along fluid trajectories in the absence of relaxation effects:

$$\begin{aligned} (\alpha_{1x})_R &= (\alpha_{1x})_R, \\ (\alpha_{1x})_L &= (\alpha_{1x})_L, \\ (\alpha_{1y})_R &= (\alpha_{1y})_R, \\ (\alpha_{1y})_L &= (\alpha_{1y})_L. \end{aligned} \quad (14)$$

The internal energy jump conditions for stiffened EOS  $p_k = (\gamma_k - 1)\rho_k e_k - \gamma_k \pi_k$ , ( $k=1,2$ ) provide the following relations:

$$p_k^* = (p_k + \pi_k) \times \frac{(\gamma_k - 1)\rho_k - (\gamma_k + 1)\rho_k^*}{(\gamma_k - 1)\rho_k^* - (\gamma_k + 1)\rho_k} - \pi_k, \quad k=1,2. \quad (15)$$

Approximate Riemann solvers (7)-(15) allow to apply described Godunov scheme. Extension to second order can be done with MUSCL type method. In this approach the predictor step is fulfilled for primitive variables with a half time interval. New values for primitive variables are used then in HLLC solver to update system (5) in corrector step.

Relaxation step for pressure non-equilibrium model can be reduced from system (6) to a couple of equations:

$$e_k \left( p, \frac{1}{\rho_k} \right) - e_k^0 \left( p_k^0, \frac{1}{\rho_k^0} \right) + p_I \times \left( \frac{1}{\rho_k} - \frac{1}{\rho_k^0} \right) = 0, \quad k=1,2. \quad (16)$$

where  $p_I$  - interface pressure, which can be evaluated as  $p_I = p$  or  $p_I = p^0$ ; superscript 0 means initial state before relaxation.

To find unknown variables:  $p, \rho_1, \rho_2$  one closure relation is needed. For this purpose saturation constraint is used:

$$\alpha_1 + \alpha_2 = \frac{(\alpha\rho)_1}{\rho_1} + \frac{(\alpha\rho)_2}{\rho_2} = \frac{\alpha_1^0 \rho_1^0}{\rho_1(p)} + \frac{\alpha_2^0 \rho_2^0}{\rho_2(p)} = F(p) = 1$$

#### IV. COMPUTATIONAL RESULTS

In all computations the liquid is governed by the stiffened gas equation of state with parameters:  $\gamma_{liq} = 2.1, \pi_{liq} = 10^7$  Pa. The gas is governed by the ideal gas equation of state with polytropic exponent  $\gamma_{gas} = 1.4$ .

**A. Round droplet**

A round water droplet with radius  $R = 0.11m$  placed in air. The pressure is  $10^5$  Pa everywhere outside the droplet. Inside the droplet the pressure is  $10^5 + \frac{\lambda}{R} = 10^5 + \frac{1000}{0.11} = 109090$  Pa according to Laplace law. The mesh with  $100 \times 100$  cells was used. The pressure profiles for initial instant and after 100000 calculation steps are shown in Fig. 1. The scheme retains the pressure jump with error which is lower than 10% comparing with the value from Laplace law.

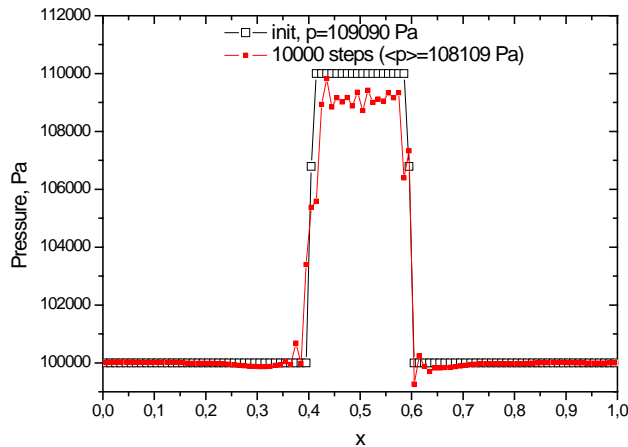


Fig. 1. The pressure profiles for initial instant and after 100000 calculation steps.

**B. Oscillating square droplet**

A square water droplet placed in air. The pressure is  $10^5$  Pa everywhere in the computational domain. The mesh with  $100 \times 100$  cells was used. The initial position of the square droplet is shown in Fig. 2 using gas volume fraction profile.

The droplet becomes to decrease its surface energy due to surface tension effects which are characterized by the parameter  $\lambda = 1000N/m$ . This induces the oscillations up to equilibrium state.

Results of calculations are presented in Fig. 3 at different instants ( $t_1 = 26ms$ ,  $t_2 = 53ms$ ,  $t_3 = 79ms$ ,  $t_4 = 106ms$ ). At steady state the droplet has a circular shape of radius 0.13 m with an average surplus pressure 7010 Pa. The error in the pressure jump is lower than 10% comparing with the value from Laplace law, which is  $\approx 7690$  Pa.

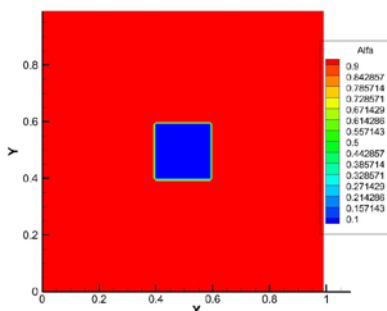


Fig. 2. Initial position of the square droplet.

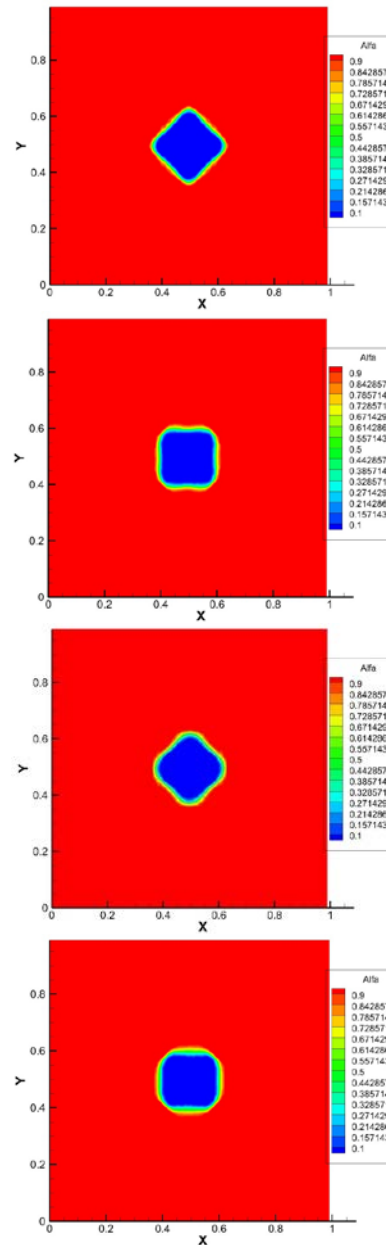


Fig. 3. Oscillation of the square droplet due to surface tension effects at different instants.

**C. Oscillating Ellipsoid Bubble**

An ellipsoid gas bubble with axis ratio 1:1.5 placed in water. The pressure is  $10^5$  Pa everywhere in the computational domain. The mesh with  $100 \times 100$  cells was used.

The initial position of the ellipsoid bubble is shown in Fig. 4 using gas volume fraction profile.

The bubble becomes to decrease its surface energy due to surface tension effects which are characterized by the parameter  $\lambda = 1000N/m$ . This induces the oscillations up to equilibrium state.

Results of calculations are presented in Fig. 5 at different instants ( $t_1 = 43ms$ ,  $t_2 = 68ms$ ,  $t_3 = 145ms$ ,  $t_4 = 183ms$ ). At steady state the bubble has a circular shape of radius 0.135 m

with an average surplus pressure 6750 Pa. The error in the pressure jump is lower than 10% comparing with the value from Laplace law, which is  $\approx 7400$  Pa.

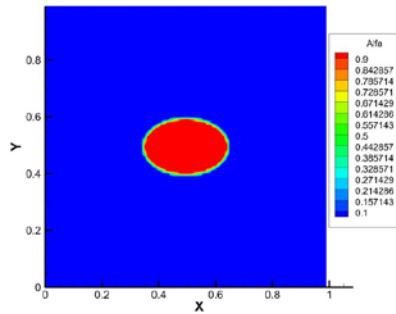


Fig. 4. Initial position of the ellipsoid bubble.

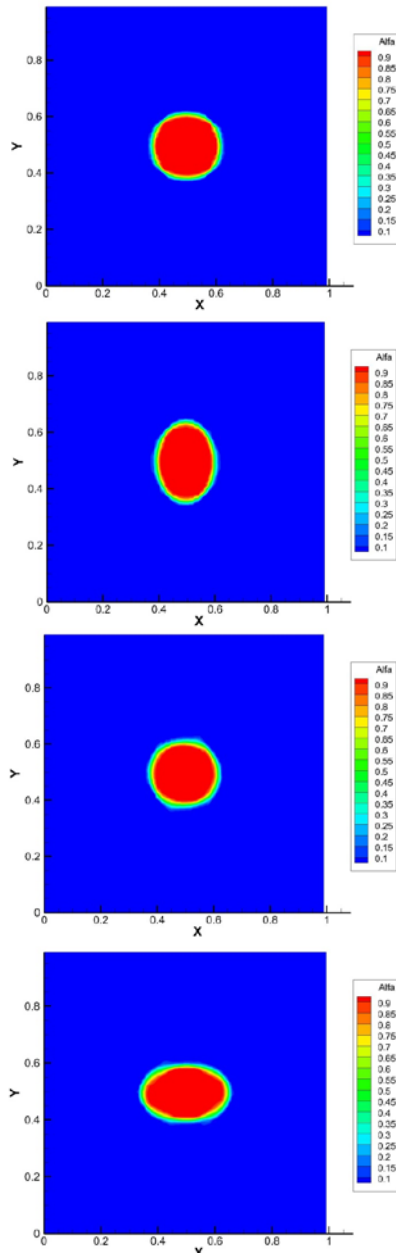


Fig. 5. Oscillation of the ellipsoid gas bubble due to surface tension effects at different instants.

#### D. Gas Bubble Surfacing In Liquid

A round gas bubble initially is placed at the bottom part of solid vertical tube, filled by the water.

The pressure profile is stratificated from  $10^5$  Pa at lowest section of the tube according to the gravity force action (see Fig. 6).

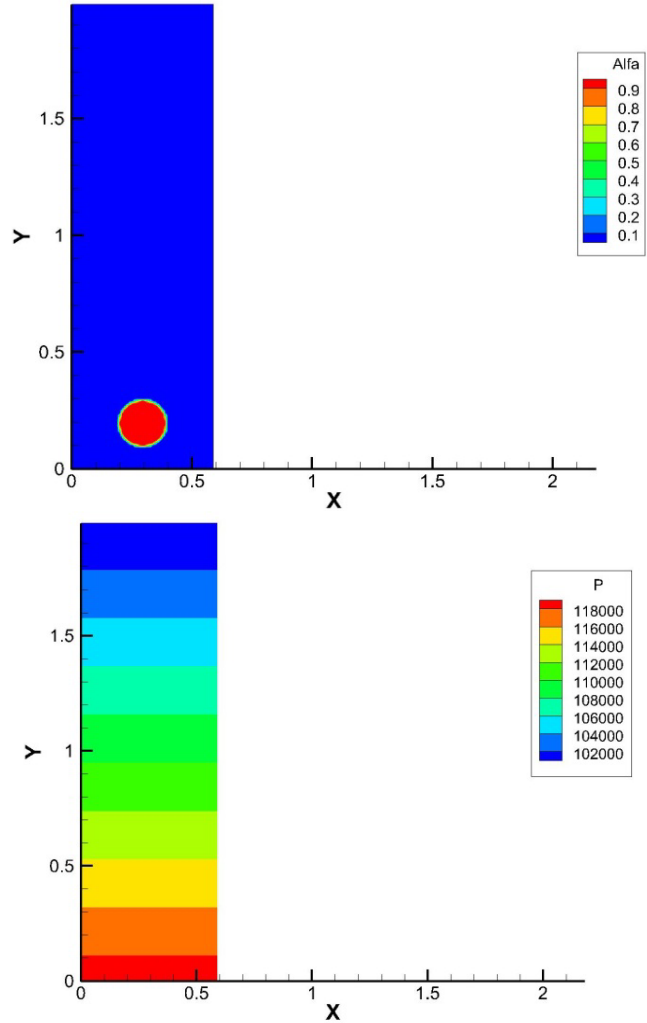


Fig. 6. Initial position of the gas bubble in solid tube (up) with stratificated profile of the pressure (down).

Gas bubble begins to surface due to the density gradient in gravity field and changes the form due to surface tension effects which are characterized by the parameter  $\lambda = 2 N / m$ .

Bubble positions at different instants ( $t_1 = 0.28 s, t_2 = 0.82 s, t_3 = 1.37 s, t_4 = 2.06 s$ ) are shown in Fig. 7 using gas volume fraction profile.

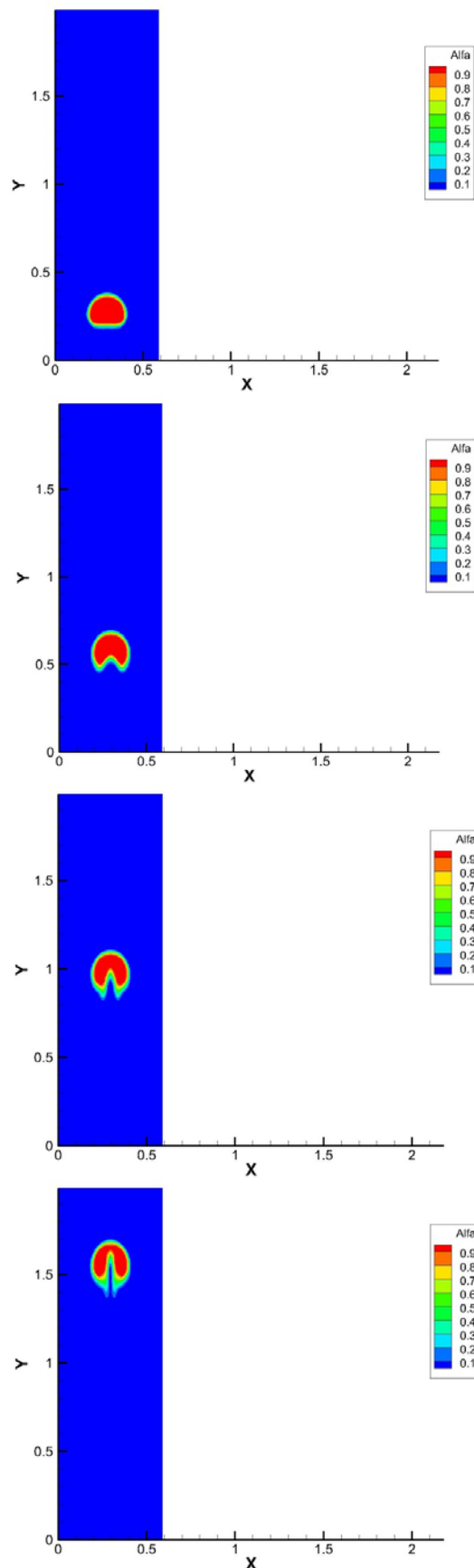


Fig. 7. Gas bubble surfacing in surrounding liquid due to the density gradient in gravity field. Bubble positions at different instants.

E. Propagation of pure capillary standing wave

A water and vapor sinusoid interface is located at the middle part of the square domain with solid walls.

The pressure is  $10^5$  Pa everywhere in the computational domain. The mesh with  $150 \times 150$  cells was used.

The initial position of the interface is shown in Fig. 8 using water mass and volume fraction profiles.

The surface tension and dynamic viscosity coefficients are  $\lambda = 1000 N / m$  and  $\nu = 6 Pa \times s$ .

The simulation results provided for pure capillary waves with viscosity effects are presented in Fig. 9 at different instants ( $t_1 = 0.16s$ ,  $t_2 = 0.29s$ ,  $t_3 = 0.46s$ ,  $t_4 = 0.59s$ ) using water mass fraction profile.

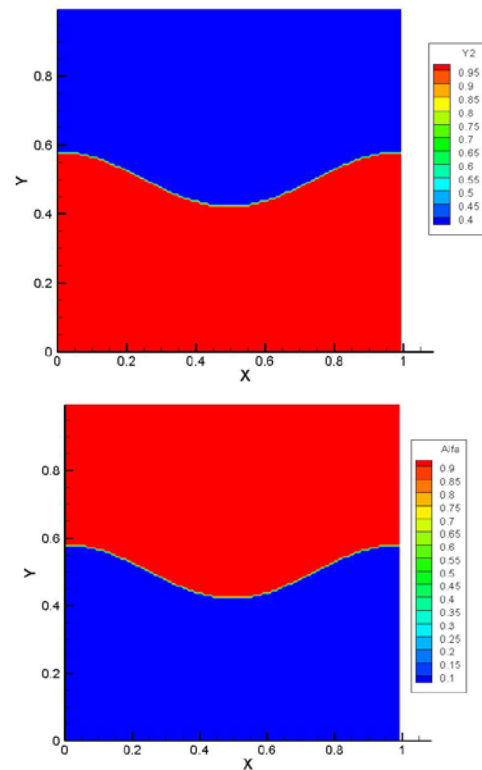


Fig. 8. Initial water mass (left) and volume (right) fraction profiles.

V. CONCLUSION

Results of testing of numerical technique speak about the good perspective of developed approach for multi-phase flow simulation.

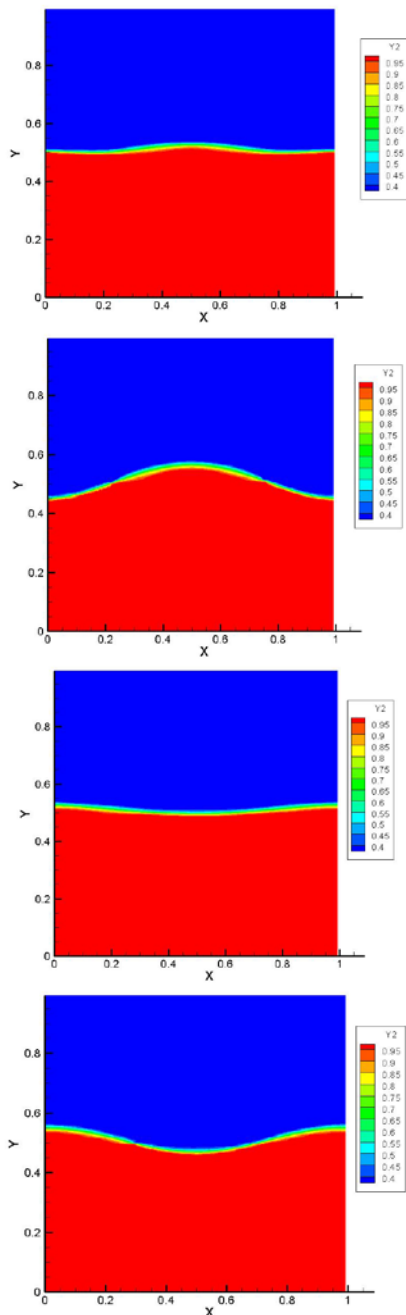


Fig. 9. Water and vapor interface oscillation due to capillary waves with viscosity effect at different instances.

#### REFERENCES

- [1] B. Lafaurie, C. Nardone, R. Scardovelli, S. Zaleski, G. Zanetti, "Modelling merging and fragmentation in multiphase flows with SURFER", *J. Comput. Phys.* Vol. 113, Issue 1, 1994, pp. 134–147.
- [2] S. O. Unverdi, G. Tryggvason. "A Front Tracking Method for Viscous Incompressible Flows", *J. Comput. Phys.* Vol. 100, Issue 1, 1992, pp. 25-37.
- [3] J. A. Sethian, *Level Set Methods: Evolving Interfaces in Geometry, Fluid Mechanics, Computer Vision, and Materials Science*, 1 Ed., Cambridge University Press, 1996.
- [4] F. Beux, B. Knowlton, S. Banerjee, "A three-dimensional level set method for direct numerical simulation of two-phase flows in variable gravity environments", *Proceedings of the 4th Microgravity Fluid Physics and Transport Phenomena Conference*, Cleveland, 1998.
- [5] D. Jamet, O. Lebaigue, J.-M. Delhay, N. Coutris, "A Numerical Description of a Liquid-Vapor Interface Based on the Second Gradient Theory", *Int. J. Fluid Mech. Res.*, 22, Issue 1, 1995, pp.1-14.
- [6] V. V. Chudanov, A. E. Aksenova, V. A. Pervichko, V. F. Strizhov, "The analysis of the large scale RCW test", *Proc. MASCA seminar 2004*, Aix-en-Provence, France. June 10-11, 2004, Vol.1, pp.217-230.
- [7] V. Chudanov, A. Aksenova, V. Pervichko, "CFD Based Numerical Modules for Safety Analysis at NPPs Validation and Verification", *J. of Mat. Science and Engin.*, Journal of Materials Science and Engineering B 1, 2011, pp. 259-267.
- [8] R. Saurel & R. Abgrall, "A Multiphase Godunov Method for Compressible Multifluid and Multiphase Flows", *J.Comp. Phys.*, Vol. 150, Issue 2, 1999, pp.425-467.
- [9] S. L. Gavriluk & R. Saurel, "Mathematical and Numerical Modeling of Two-Phase Compressible Flows with Micro-Inertia", *J. Comput. Phys.* Vol. 175, Issue 1, 2002, pp. 326-360.
- [10] E.F. Toro M. Spruce and W. Speares, "Restoration of the Contact Surface in the HLL-Riemann Solver", *Shock Waves*, Vol. 4, No. 1, 1994, pp. 25 – 34.
- [11] R. Saurel, F. Petitpas, R. A. Berry, "Simple and efficient relaxation methods for interfaces separating compressible fluids, cavitating flows and shocks in multiphase mixtures", *J. Comput. Phys.*, Vol. 228, Issue 5, 2009, pp. 1678-1712.
- [12] R. A. Berry, R. Saurel, F. Petitpas, E. Daniel, O. Le Métayer, S. Gavriluk, N. Dovetta, R. C. Martineau, "Progress in the Development of Compressible, Multiphase Flow Modeling Capability for Nuclear Reactor Flow Applications", *INL Report*, No. INL/EXT-08-15002, 2008, pp. 143-168.